Anomaly classification by inserting prior knowledge into a max-tree based method for divertor hot spot characterization on WEST tokamak

Valentin Gorse, Raphaël Mitteau, Julien Marot

Anomaly classification by inserting prior knowledge into a max-tree based method for divertor hot spots characterisation on WEST tokamak

Valentin Gorse,[1, a)] Raphaël Mitteau,[1] and Julien Marot[2]
[1)] *CEA, IRFM, F-13108 Saint-Paul-Lez-Durance, France*
[2)] *Aix-Marseille Université, CNRS, Ecole Centrale Marseille, Institut Fresnel, 13013 Marseille, France*

(Dated: 8 August 2023)

The divertor of WEST (W Environment in Steady-state Tokamak) is the main component for plasma control and exhaust. It receives high heat fluxes, which can cause damage to plasma facing units above the allowable heat flux. Improving the operation safety on the actively cooled tungsten divertor is being researched in place at WEST, toward providing divertor monitoring solution for ITER. Divertor operation safety relies on detecting, monitoring, and classifying all hot spots on the divertor surface using infrared (IR) cameras. In this paper, a method based on max-tree representation and attributes of IR images is used to classify normal from abnormal strikelines on the divertor. The proposed method requires only high-level prior knowledge of abnormal temperatures and divertor structure but does not require any labelled data, unlike existing methods such as support vector machines (SVM) or convolutional neural networks (CNN). The max-tree classifier method is tested on real IR images from the WEST tokamak and shows that 88% of hot spots are accurately classified with a small enough calculation duration, that can be performed between two pulses.

I. INTRODUCTION

Tokamak fusion plasmas endeavour to achieve the fusion of Deuterium (D) and Tritium (T) atoms, which holds great potential as a future energy source. Tokamaks have demonstrated increasing power capabilities, with the tokamak JET achieving fusion outputs of 20 to 40 MW and International thermonuclear experimental reactor (ITER) projected to reach up to 500 MW. The magnitude of power used or generated by these facilities categorizes them as large-scale industrial installations. Furthermore, there is a growing tendency among magnetic fusion devices towards continuous plasma operation, ranging from several minutes to hours, with energy throughputs comparable to those of substantial power plants. For example, WEST (W Environment in Steady-state Tokamak)[1] operates routinely with 4 MW of power, for a plasma duration over a minute (record of 6 minutes, Tore Supra (WEST Tokamak predecessor) in 2004). Figure 1(a) gives an overview of the interior of the WEST Tokamak, showing the main plasma facing components acting as thermal shield, and especially the divertor at the bottom of the machine.

The large amounts of power and energy involved are evacuated through the walls, acting as thermal shields. They operate in a stationary manner with surface temperatures of 500 to 1000°C. In addition to the normal power evacuation, which must be monitored, parasitic phenomena (magnetic instabilities, additional heating power losses) send occasionally hot plasma to undesirable locations, resulting in potentially damaging hot spots and thermal events. These phenomena are monitored for optimal machine operation, and sometimes require counter-reaction or other safety actions.

Active temperature control of Plasma facing components during plasma operation is an increasing trend among tokamaks/fusion machines, especially as plasma discharge duration extends and overcome thermal stabilisation time constant. Active temperature feed back control is for instance done in WEST tokamak in south of France but also in JET tokamak[2] in the United Kingdom, EAST tokamak in China[3] or Wendelstein 7-X (W7-X) stellerator in Germany[4]. W7-X research collaborators are also working on automating infrared image analysis to address machine safety concerns. W7-X investigated the feasibility of employing the max-tree method for automatic segmentation of hotspots[5,6].

Connected operators are predominantly utilized for image filtering or image segmentation. The application of these methods is widespread in various domains of image analysis, including but not limited to medical applications for example. Although rare, there have been instances where this method has been employed for classification purposes[7]. This article presents a novel implementation of classification on infrared images using connected operators.

This article describes the current state of WEST tokamak technology toward active wall temperature control, and the architecture of the infrared diagnostics data processing toward this goal.

This article addresses the challenge of hotspot classification, with a special focus on the identification of anomalous strikelines. A novel classification methodology on infrared imagery acquired from cameras installed within the tokamak is proposed.

This article is organized as follows. Section II describes the instruments and issues involved in the research, including the IR diagnostics installed on the WEST tokamak and a description of the relevant hot spots and ther-

[a)]The author to whom correspondence may be addressed: valentin.gorse@cea.fr

mal events. Section III outlines the max-tree classifier methodology for strikeline classification using the max-tree image processing method, resulting into a sorting of the wall hot spots into individual branches. The approach to cut the branches of the resulting tree and the criteria to determine such a classification are also presented and discussed. Section IV reports on the findings including metrics and comparative methods as well as numerical results. Finally, section V discusses the limits of applicability of the research including an examination of physical parameters thanks to a synthetic dataset and some practical cases not detected by the max-tree classifier method. The article concludes by highlighting the importance of continued research in this area to ensure the safe and efficient operation of tokamaks as a source of energy.

The following notations are used throughout the paper:

$\{A_1\}$ symbolises a node of the tree generated by the max-tree method. This node is composed of all the pixels in the area associated with the letter. The index gives the grey level associated with the area.

$\mathbb{P}$ symbolises a probability distribution, μ and σ correspond respectively to the mean and standard deviation of the distribution.

All the IR images use the "Hot" colormap, the interval given for the colormap is from the temperature of the darkest point to the temperature of the brightest point.

II. MATERIALS

A. IR diagnostics installed on WEST tokamak

Infrared camera-based optical measuring instruments are employed to monitor the thermal shields during operation, providing armour surface temperatures. Approximately 50% of the whole internal wall is observed by optical systems, while the rest is monitored passively or indirectly. The system features 12 IR cameras mounted on seven optical endoscopes positioned in the machine's upper ports with downward-facing views. This configuration provides comprehensive coverage of the lower divertor, baffle leading edge, and five heating devices: three Ion Cyclotron Resonance Heating (ICRH) antennas and two Lower Hybrid Current Drive (LHCD) launchers. Additionally, new optical viewing systems have been developed for WEST, including a wide-angle tangential view of the inner chamber from an equatorial port (Figure 2(a)); a high-resolution view of the divertor with 0.1 mm spatial resolution; and two complementary views of the divertor (direct view through a window, scheme on Figure 1(b)). This entire acquisition system is described by Courtois et al. in[8].

A complete chain of measurement and acquisition is functional: conversion from raw digital levels to temperature, acquisition, storage, and access to data[9,10]. Expert analysis of hot spots by human operators takes into account many parameters, such as their shape, extent, possible structure, temperature value, and temporal correspondence with other machine events. In addition to data accessible by direct or indirect measurements, the analysis of hot spots is based on historical knowledge of past thermal events and synthetic images produced from first principle physical models (digital twins).

In addition to the human expertise, automated infrared data processing has been developed at the IRFM Infrared laboratory for over a decade. Initial methods were purely quantitative with fixed thresholds alerting safety experts based on involved area/materials. Subsequently, more "intelligent" image analysis incorporating classification techniques linked to hotspot shape/size/duration emerged as detailed in[11].

Real-time monitoring is implemented using images from infrared cameras in the Wall Monitoring System (WMS)[12], with temperature thresholds defined according to components allowable. Control laws are implemented to monitor and feed back on actuators if control thresholds are exceeded. These basis controls are in use today, but they are exceedingly basic, and subject to false positive[12].

More elaborated controls using artificial intelligence and deep learning are investigated. An end-to-end pipeline is developed to detect and classify hot spots[13,14] based on recognisable features like hot spot shape, position, and temperature distribution, possible combined. The classification method described in this article is part of this data pipeline and is aimed at consolidating the accuracy of detection / classification on hot spots detected by artificial intelligence.

Infrared cameras are employed in various disciplines for non-destructive evaluation through thermographic techniques. Additionally, several methods[15,16] have been developed to facilitate the automatic identification of specific anomalies. In contrast to many applications where the nature of the defect is predetermined and the input data is relatively unambiguous, monitoring the heat shield of tokamak walls presents a unique challenge.

B. Hot spots description and related issues

The issue of monitoring the machine is linked to the presence of hot spots on the tokamak's walls. There are various types of hot spots, including "strikelines", "electron type 1", "ripples loss" or "Unidentified Flying Objects" (UFOs), which may result from the pulverisation of wall armour and subsequent detachment of metal dust. The full taxonomy is much more extended than described above, a reduced taxonomy is used currently and proves efficient for development activities[13]. In the previous subsection, various infrared image analysis techniques are described. These techniques are employed to detect and classify the different types of hot spots present in the WEST tokamak, thereby ensuring its safe operation.

The "Strikelines" are the most common hot spot be-

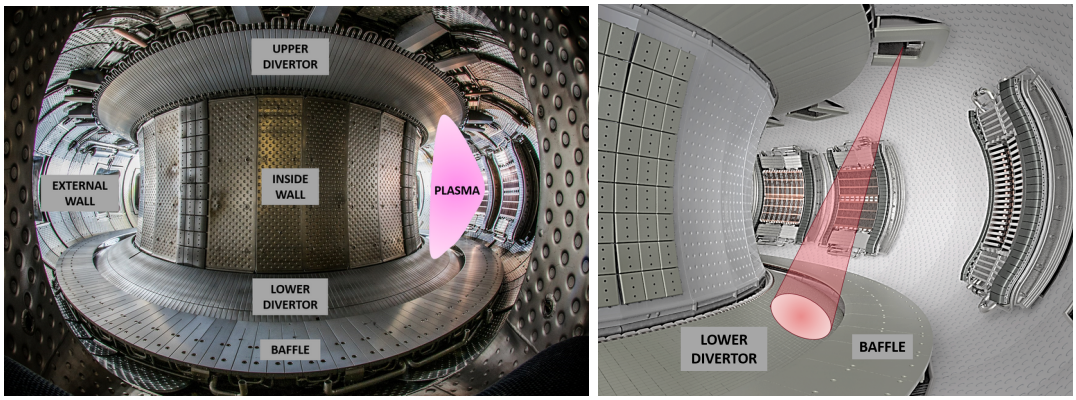

(a) (b)

FIG. 1. Photo of the interior of the WEST Tokamak including some areas description (a). Simplified 3D reproduction of the tokamak with a divertor sight-of-view IR camera (b).

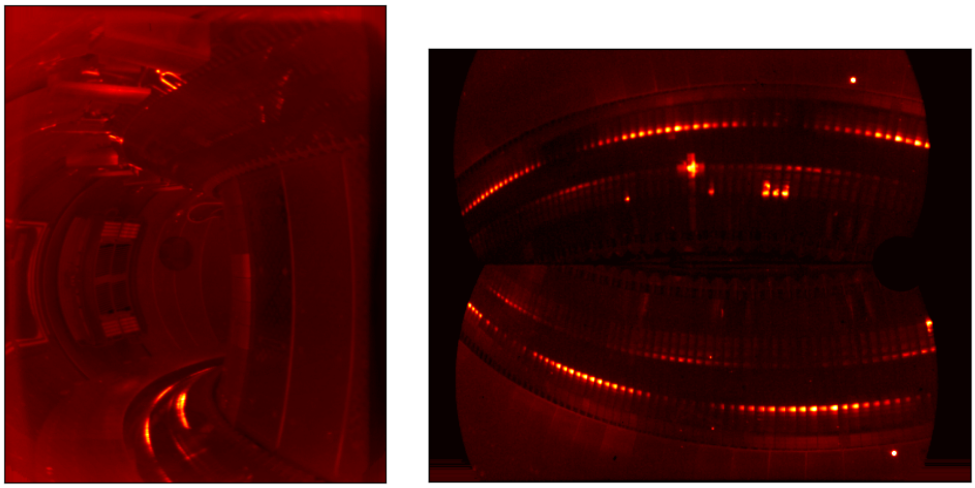

(a) (b)

FIG. 2. Wide Angle (WA) camera (a) & Line of sight of a divertor camera (DIVQ1B) (b) for pulse 57541. Hot colormap for (a): [108°C;256°C] and for (b): [91°C;462°C]

cause they result from the normal power deposition on the divertor (top or bottom). The physical justification to strikeline is explicated in[17], in particular with Figure 5.4 at page 217 showing a toroidal cut-out of a tokamak with the contact zone between the outer plasma layer and the divertor.

Figure 2(b) presents an infrared image of the lower divertor during a pulse. The lower half of the image is an extension of its upper region: due to the divertor's large aspect ratio along the entire length of the tokamak, capturing a 60° sector within a single field of view makes a poor usage of the detector. Two lines of sight and a recombination prism are used to better fit the FoV of a 60° divertor sector within the detector.

As depicted in Figure 2(b), these lines are not continuous and exhibit a sinusoidal modulation because of the discrete arrangement of the 18 toroidal magnetic coils on the WEST tokamak (the so-called "ripple effect"). Strikelines exhibit a characteristic "croissant" shape, with a series of local hotter spots resulting from the series arrangement of plasma facing units. The hottest spots are concentrated towards the centre of the strikeline. This physical knowledge facilitates differentiation between a "normal/classical" strikeline and an abnormal strikeline that warrants priority monitoring. Normal strike lines have a temperature per Plasma facing Unit (PFU), which temperature peaks are grouped together (the temperature of these PFUs for a strikeline without anomalies is called "normal" temperature in the rest of the article). By contrast, a defective strike line has one or two peak temperatures deviating significantly from the grouped temperature of the other fingers.

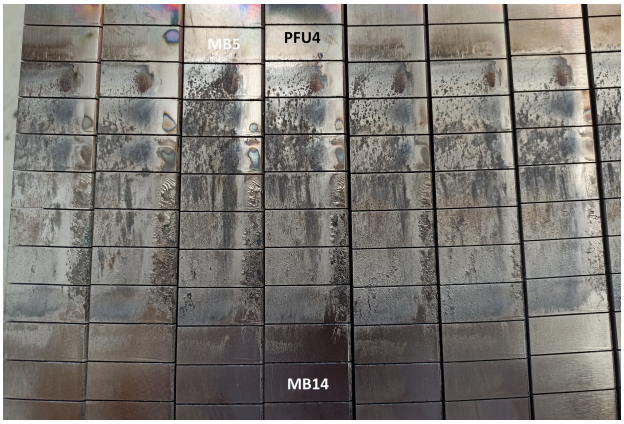

FIG. 3. Photo of WEST divertor (Q1A) from PFU 1 to 8 after C7 campaign. The strikepoint between plasma and Divertor is located on monoblock (MB) 16.

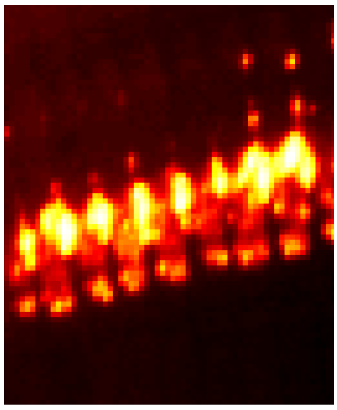

FIG. 4. Abnormal strikeline due to some deposit spotted during the WEST tokamak operation campaign in April 2023. (58500 - DIVQ6B - "Hot" Colormap (exceptionally non-linear for a better visualisation): [100°C;360°C])

Abnormal PFU temperatures originates from several possible causes: deteriorating thermal contact to the cooling circuit, growth of a resistive thermal deposit at the surface of the armour tile, or possible a tile or PFU misalignment, either pre-existing or happening following fixture deterioration of the PFU.

Further temperatures anomalies may happen because of erosion or dust deposition on the divertor. When tungsten blocks are damaged to a degree that their outer layers are altered, it is possible for the emissivity of the material to change, thereby altering the apparent temperature obtained by the IR camera. Similarly, dust deposits on a machine in the field of view can accumulate on the divertor at ground level and modify the emissivity of certain zones, resulting in abnormal strikelines. These phenomena can be observed when the divertor is studied after an experimental campaign (see Figure 3).

Misalignment of one or more Plasma Facing Units (PFUs) is another factor that can result in the observation of an abnormal strikeline and require close monitoring of the affected area. Vertical misalignment of PFUs poses a significant challenge in such machines as the accepted tolerance is only 0.3mm[18]. Precise alignment of the divertor is crucial for it to effectively perform its heat absorption function. A misaligned PFU results in overexposure of its leading edge and consequent abnormal heating along its entire length. Furthermore, significant misalignment of a PFU casts a 'shadow' on the adjacent unit due to their 'staircase' arrangement.

Figure 4 depicts a strikeline that may be considered abnormal by a human expert due to its unexpected shape and temperature differences between certain areas. This Figure 4 is the infrared counterpart of Figure 3, during the end of C7 campaign. The max-tree classifier method described in this article aims to detect such atypical strikelines and promptly alert the safety officer of the first wall after the pulse.

III. METHOD

The section III outlines the development of a classification method, from the creation of a synthetic dataset to the selection of appropriate classification criteria.

A. Synthetic image creation

While it is feasible to address this issue solely through experimental data, the process of annotation can be time-consuming. Consequently, generating a synthetic image dataset with easily verifiable labels and anomaly types (if present) presents a compelling alternative. Utilizing synthetic data enables more comprehensive analysis of max-tree results on images of this nature, facilitating the identification of pertinent criteria for anomaly classification. The process involves several steps:

1. A 1D profile of heat flux and temperature distribution on the surface of a PFU monoblock is generated using CAST3M[19] thermal calculation code from physical input parameters from the WEST tokamak.

2. Monoblocks and their temperature distribution are multiplicated horizontally to generate a 1D line with N monoblocks. The physical gap present on the WEST divertor is added between each monoblock by artificially inserting points at 70°C (machine base temperature). This horizontal (X) direction serves later as 'toroidal' direction.

3. The 1D line is developed vertically to create a 2D image of N PFUs with identical distribution along the entire vertical and repeated patterns between all monoblocks. The vertical axis serves later as poloidal direction.

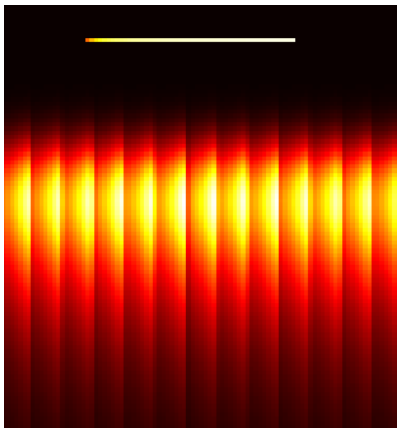

FIG. 5. Example of a synthetic strikeline ("Hot" colormap: [70°C;237°C])

4. Gaussian and Eich[20] flux distribution laws are applied on toroidal and poloidal axes respectively to impose toroidal field ripple modulation around tokamak and flux intensity at plasma-PFU contact.

5. A pixel/cm filter matching the resolution of IR cameras defined in[8] is applied.

Images with anomalies are generated by deliberately misaligning one PFU before CAST3M simulation resulting in new flux distribution on two PFUs (misaligned one and shaded one). The images generated through this process enable the correlation of hot spot emergence with specific physical events, such as the misalignment of a PFU. An example of a generated artificial strikeline is provided in Figure 5.

It is chosen to generate the artificial image database, using the misalignment cause as a parameter. Direct modelling of defective strike line having a larger temperature because of the misalignment is representative of the abnormal strike lines. A total of 1350 synthetic images were generated by varying three parameters: the vertical misalignment (in mm), the number N of PFUs in the image and the anomaly position. The utilization of synthetic images contributes to the formulation of criteria delineated in subsection D.

B. Image pre-processing

The image process at the core of the technique is built upon a max-tree transform of the image. The next subsection introduces the max-tree image processing method. The images are quantized into discrete temperature levels. For this quantization, the temperatures are grouped into bins of 5% of T_{max}. The value at the median of its interval is assigned to each bin. Image quantization reduces the number of levels in an image by compressing a range of values to a single value. Quantization is a mandatory processing step, else the max-tree process would result in exceedingly numerous digital levels, which would hinder proper recognition of graph branches. The quantization is also justified by two physical arguments:

- The infrared camera used on WEST do have a finite measurement uncertainties, which make it irrelevant to decompose the image at the Celsius degree level.

- A quantized image reveals better the essential information about the physical structure and the temperature contrast between different regions.

C. Max-tree operation principle

Salembier et al.[21] proposed max-tree as a hierarchical data structure that captures the topological and morphological properties of a grey-level image. In this representation, the root node corresponds to the background of the image and contains all the pixel indexes with the minimum grey-level value. The intermediate nodes correspond to different connected regions of pixels with increasing grey-level values. The leaf nodes correspond to the regional maxima of the image, where no pixel has a higher grey-level value in its neighbourhood.

The algorithm works by creating a "local" background at each temporary TC_h^k node, which consists of all pixels with a grey level value of h (the "local" background may not be a single piece). Then it finds the connected regions of pixels with a grey level value above h and makes them the child nodes of the tree. During this process, the algorithm may create some nodes that have no pixel in them. These nodes are deleted after the tree is built. The final tree is called a max-tree because it shows the image's highest values (the highest values are at the end of the tree branches) and gives a "tree-like" representation of the image, which is also a reduced size data format that preserves the structure of the image.

The algorithm is explained here in details. It is applied it to a model image of a strikeline, shown in Table I. This idea of explanation from a simplified is derived from[21],[22] or[23]. The example image has 9 connected components (A-I) spread over four grey levels (0 to 3). The algorithm starts with the lowest grey-level (0) as a threshold value and assigns pixels of $\{A\}$ with this value to the root node C_0. The remaining pixels are divided into two connected components ($\{B, C, D, E, F, G, H\}$ and $\{I\}$) and assigned to temporary nodes: $TC_1^1 = \{B, C, D, E, F, G, H\}$ and $TC_1^2 = \{\mathrm{I}\}$. Table I(a) shows the result of this iteration. In the next iteration, the threshold is increased by one and each temporary node is processed separately. For example, TC_1^1 contains one connected component with grey-level 1 : $\{B\}$ and three connected components with higher grey-levels ($\{C, F\}$,$\{D, G\}$ and $\{E, H\}$). The pixels of B are assigned to a new node and added to the tree, while the pixels of $\{C, F\}$,$\{D, G\}$ and $\{E, H\}$ are assigned to new temporary nodes. Table I(b) illustrates this step. The

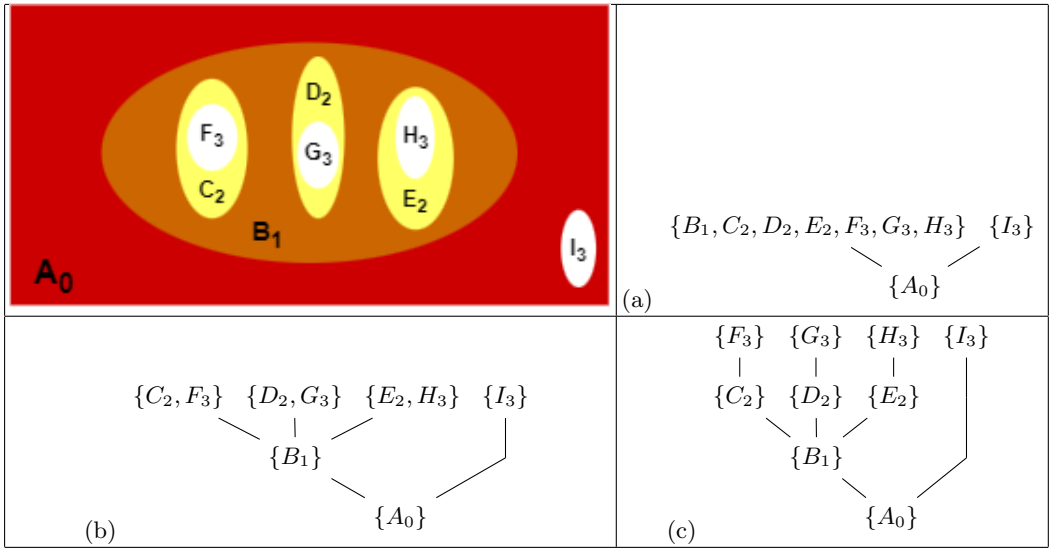

TABLE I. Example of a very simplified strikeline with 4 temperature levels. The letters represent the different zones of the image and the numbers represent temperature levels. Max-tree creation process. (a), (b) and (c) are respectively the first, second and third iteration of the creation process.

algorithm continues until all pixels are assigned to nodes in the tree. Empty nodes are then removed from the tree to obtain the final max-tree representation shown in Table I(c).

With regards to implementation, the calculation of the max-tree method can be achieved using three distinct groups of algorithms. In an effort to remain consistent with the ideas presented in[21], a flooding algorithms is selected for use[24].

D. Cutting the branches of the resulting tree

Anomaly detection in images represented as directed trees can be achieved by analysing the branches associated with the highest temperature values. The selection criterion is applied to these upper branches. It is based on a common temperature threshold that allows us to compare the dimensions and shapes of the selected branches:

1. Find the maximum temperature of each branch.
2. Compute the mode of the maximum temperatures across all branches.
3. Set a threshold at 75% of the mode value.
4. Cut all branches at the threshold value.

Therefore, the tree is pruned by removing all the nodes below this threshold.

This method presents several advantages over prescribed thresholds. Firstly, it operates independently from varying power levels injected into the tokamak, which results in many possible hot spot temperatures. Secondly, it is robust to potential anomalies aimed to be detected, as it relies on the most frequent maximum temperature of the strikeline, which is also the regular PFU temperature. This choice of threshold (75%) is the first integration of a priori knowledge in the method. The precise value of the threshold affects mostly what is defined as the boundary and contour of a hot spot, which remain anyway an open matter in wall monitoring activities. Thus, it was decided to consider that the hot zone of interest for these strikelines is delimited by temperatures above 75% of the "normal" temperature. This choice represents a progress over a fixed or proportional threshold, that would be used to reveal hot spots.

After applying the tree pruning, B branches were obtained with N_b pixels each. The number B varies between 7 and 15 depending on the plasma configuration. The number of pixels within the branch N_b (with $b = 0, 1, ..., B-1$, index of the branch) is widely variable, as it can be very small (e.g., one very hot pixel due to a camera defect) or very large (e.g., a complete PFU heating). The size of each branch is a controlling parameter for determining whether a branch represents an anomaly or not: for example, a branch with a unique pixel is a bad pixel, not a hot zone on the divertor.

E. Classification criteria

Identifying anomalies in the image requires establishing appropriate criteria that are effective to distinguish normal from abnormal branches based on their thermal properties. These criteria are based on a priori knowledge of the strikelines. Three criteria are proposed to be

used in a similar pattern. Physical prior knowledge enables the understanding of the expected behaviour of a "normal" strikeline. Thus, a branch, representing a part of the global hotspot, that does not exhibit certain expected characteristics can be extracted. These are the three criteria used:

- **Maximum temperature of the branch**: The first intuitive criterion for anomaly detection is the maximum temperature of each branch denoted by T_{max_b} for branch b. This reflects the human safety expert's concern for the thermal state of the component and the potential risk of overheating. Prior physical knowledge indicates that the maximum temperatures along the strikeline hot zones are within a relatively close range of temperatures. The "3σ rule" is applied to detect outliers in this distribution.
  $\mathbb{P}(\mu-3\sigma \leq T_{max_b} \leq \mu+3\sigma) \approx 0,9973$ so any branch with a maximum temperature too high compared to the rest (*i.e*, more than $\mu + 3\sigma$) is considered as an potential anomaly and marked for further analysis. For example, in circumstances where the entirety of a strikeline maintains a temperature of 300°C and a singular block exhibits a temperature of 305°C, it is not cause for concern. However, if the strikeline temperature is approximately 200°C, this same block (at 305°C) may indicate an anomaly.

- **Size of the branch**: This criterion corresponds to the number of pixels of each branches. The "3σ rule" is also applied to this criterion to check for outliers in the list of branch sizes. The criterion under consideration requires not only an understanding of the strikeline's physical properties but also an awareness of potential anomalies on the divertor. As detailed in section II, the strikeline's structure is well-defined and the size of hot zones which compose the "croissant" are relatively consistent. In the absence of anomalies, branches should be approximately equal in size. However, factors such as the superposition of a UFO to the usual strikeline temperature pattern disrupts this uniformity by creating a "hot and thin" branch with few pixels in max-tree due to its significantly smaller size relative to the strikeline.

- **Temperature distribution within the branch**: In order to illustrate this criterion, the temperature is plotted as a function of the pixels for each branch, resulting in curves like those shown in Figure 6.

  The similarity in shape among most of the curves can be attributed to the structure of the tokamak and the plasma shape, which results in approximately the same temperature distribution in the "croissant" hot zones. For example, the curves drawn on (a) correspond to a normal strikeline, while the curves drawn on (b) correspond to a strikeline with a misaligned PFU. In this figure (b), the blue curve represents the branch linked to the misaligned PFU. A hotter zone is observed (the value at pixel 0 is much higher than the rest), and it is also noticeable that the decrease in temperature to reach the branch cutting threshold is much slower.

  To quantify this difference in shape, the Euclidean distance between each pair of curves is calculated. The "3σ rule" is then used to detect outliers in this distance list. A branch exhibiting a distance defined as an 'outlier' relative to (at least) half of the other branches is identified as a potential anomaly.

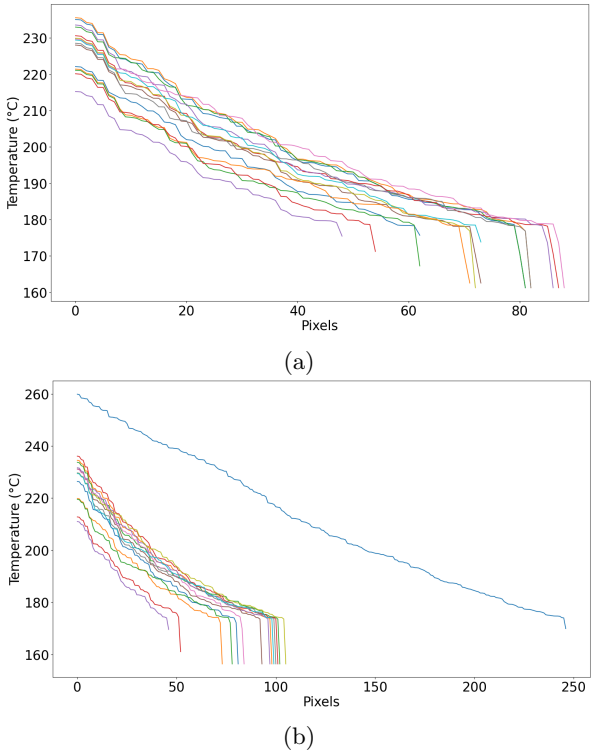

FIG. 6. Temperature distribution as a function of the number of pixel for a "normal" strikeline (a) and a strikeline with an anomaly (b). Each curve with a given colour represents the distribution of a given branch.

A branch is defined as an anomaly for the wall safety function if it is designated as a potential anomaly on at least two out of the three criteria defined above: T_{max_b} for each b, size and distribution. In the event of a potential anomaly, it is directly reported to the first wall's safety officer.

The ease of obtaining the maximum temperature of the branch classified as anomalous is an additional benefit of this method. Extra relevant information about hot spot anomaly size can be conveyed. This branch size is often key in characterising the nature of the anomaly.

From a practical standpoint, the max-tree classifier method (called "max-tree classifier" in the following text)

can be implemented between the detection of strikelines by the AI data processing pipeline[14] and the uploading of information to the institute's shared databases. The max-tree classifier adds several pieces of information, such as the presence or absence of anomalies and possibly the temperature of anomalies, to the existing data for later analysis.

IV. RESULTS

A. Metrics

In evaluating the performance of the max-tree classifier for a binary classification problem, several metrics are utilized, including Accuracy, Recall, Precision, and F1-Score. All these metrics are extracted from the confusion matrix where a Negative is defined as "non anomaly" and a Positive as an "anomaly".

- Confusion matrix: Comparison of actual and predicted class. Table II explains the content of the confusion matrix for a binary classification problem.

Classes	**Actual 0**	**Actual 1**
Assigned 0	True Neg. (TN)	False Neg.(FN)
Assigned 1	False Pos. (FP)	True Pos. (TP)

TABLE II. Definition of the confusion matrix content

- Accuracy: Computes the proportion of well-classified samples (Eq. (1)).

$$Accuracy = \frac{TN + TP}{TN + TP + FN + FP} \tag{1}$$

- Recall: Computes the fraction of relevant instances that were retrieved (Eq. (2)).

$$Recall = \frac{TP}{TP + FN} \tag{2}$$

- Precision: Computes the fraction of relevant instances among the retrieved instances (Eq. (3)).

$$Precision = \frac{TP}{TP + FP} \tag{3}$$

- F1-score: Computes the harmonic mean of the precision and recall instances (Eq. (4)).

$$F1\text{-}score = \frac{2TP}{2TP + FP + FN} \tag{4}$$

B. Comparative methods

Two alternative anomalies classification methods are used as reference benchmarks, a Convolutional Neural Network (CNN) method and a Support vector machines (SVMs). Both approaches require that the dataset under analysis contains images of identical dimensions. While this is not a concern for the max-tree method, which operates independently of image size, it is imperative from a technical implementation standpoint that all input images possess the same dimensions. Accordingly, the largest image within the dataset, measuring 95×268 pixels, is selected as the reference dimension. The dimensional increase is done by a third order spline interpolation. Consequently, the 3D matrix representing the 218 real image dataset for comparative methods has a dimensions of $\mathbb{N}^{218\times95\times268}$. For the following two methods, the dataset is split into train, validation and test sets, following the conventional approach.

1. Convolutional Neural Network (CNN) method

These images are normalized based on the statistics (mean and standard deviation) of the training set to prevent data leakage. Due to the scarcity of data, a very simple CNN is designed as shown in Figure 7. This structure is standard for a CNN and is inspired by the various advances in the field[25](structure similar to AlexNet[26] for example).

The loss function used is the binary cross entropy (L_{BCE}) defined by Eq. (5):

$$L_{BCE} = -\frac{1}{n}\sum_{i=1}^{n}(Y_i log(\mathbb{P}(Y_i)) + (1 - Y_i) log(1 - \mathbb{P}(Y_i))) \tag{5}$$

Y_i is the actual value (here, for a binary classification case: 0 or 1) where i is the index running through the size n of the dataset to be evaluated. $\mathbb{P}(Y_i)$ is the probability associated with this value (computed by the neural network).

This loss is sensitive to the distance between the predicted probabilities and the actual labels, which can help the model learn faster and avoid overfitting.

2. SVM method

Support vector machines (SVMs) are a class of machine learning algorithms that aim to find an optimal separating hyperplane for different classes of data points in the training set[27]. The optimal hyperplane is defined as the one that maximizes the margin between the classes, which is equivalent to minimizing a bound on the generalization error of the model. This approach follows the principle of structural risk minimization (SRM). In this subsection, the investigation focuses on how SVMs can classify the anomalies of the strikelines.

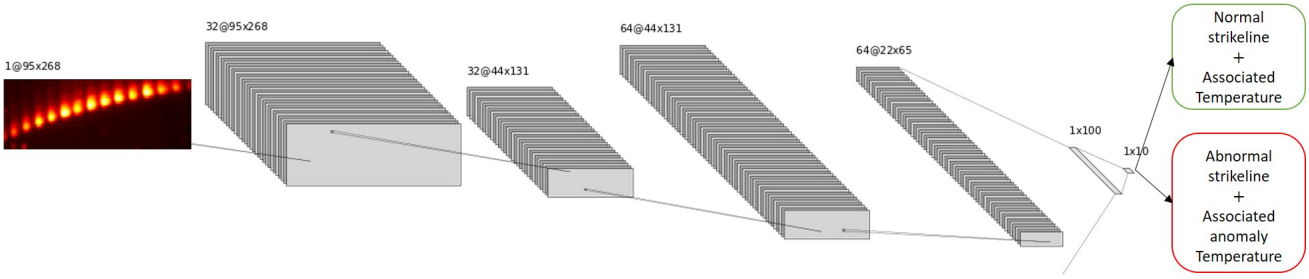

FIG. 7. CNN model used for comparison.
The layers are respectively Convolution 2D (32 filters with kernel of size 3×3), Max-Pool 2D (3), Convolution 2D (64 filters with kernel of size 3×3), Max-Pool 2D (3), Dense layer (100 neurons, ReLu activation), Dense layer(10 neurons, ReLu activation), Dense layer (2 neurons, Softmax activation) .

	Actual non anomaly	**Actual anomaly**
Assigned non anomaly	155	12
Assigned anomaly	14	37

TABLE III. Confusion matrix with max-tree method on the whole set of annotated real data

	R	S	RS
Accuracy	**0.88**	0.82	0.82
Precision	**0.73**	0.91	0.90
Recall	**0.76**	0.89	0.88
F1 score	**0.74**	0.90	0.89

TABLE IV. Statistics on the entire real-world image dataset (R), on the entire synthetic dataset (S) and on the mix of entire real-world image AND simulated dataset (RS).
(R) is composed by 218 images, (S) by 1350 and (RS) by 1568 images.

From a technical standpoint, the two-dimensional images are straightened in the form of a $1 \times N$ matrix, where N represents the number of dimensions of the vector. It results into an input matrix with dimensions $\mathbb{N}^{218\times1\times25460}$.

A linear kernel is used for this SVM. This means the decision boundary between classes is a straight line (or hyperplane in higher dimensions). Linear kernels are often used when the data is linearly separable or when the number of features is large compared to the number of training examples which is the case here ($25460 >> 218$).

C. Numerical results

1. Max-tree method results on the entire real data set

The max-tree classifier is applied to the entire labelled real IR images data set and a complete dataset with all the real and synthetic images, without requiring any training set as with other approaches. The confusion matrix (computed on the real data) in Table III shows the performance of the max-tree classifier.

The different metrics described above are derived from this confusion matrix. There are summarized in Table IV.

The max-tree based method achieved good and balanced results on detecting anomalies on real WEST tokamak strikelines (see examples of good classification of real images in Figure 8). A high recall is crucial for ensuring the safety of the machine, as it is important to minimize the number of false negatives that could lead to undetected faults. When evaluated on the complete dataset comprising both real and simulated images, the performance of the max-tree classifier improves significantly. The simulated images are "cleaner", resulting in more distinct branch cutting and a substantial increase in recall and precision.

However, since the max-tree based method is new and has not been applied to other tokamak or IR datasets, it cannot be compared with existing state-of-the-art methods for hot spot anomaly classification. As already introduced above, the max-tree classifier method is benchmarked to CNN and SVM.

2. Comparison results

This section presents an analysis of the results obtained on the test set, which comprises a subset of 218 labelled images. The max-tree method was evaluated on the same test set as other methods that require training data to ensure a fair comparison of performance.

As can be seen from Table V, the max-tree method outperforms by far all other methods on the test dataset. It attains the highest scores for accuracy (0.87), recall (0.89) and F1-score (0.73), and a satisfactory score for precision (0.62). This suggests that it can correctly classify most of the images, identify most of them that are anomaly, discard most of them that are not, and preserve a good balance between precision and recall.

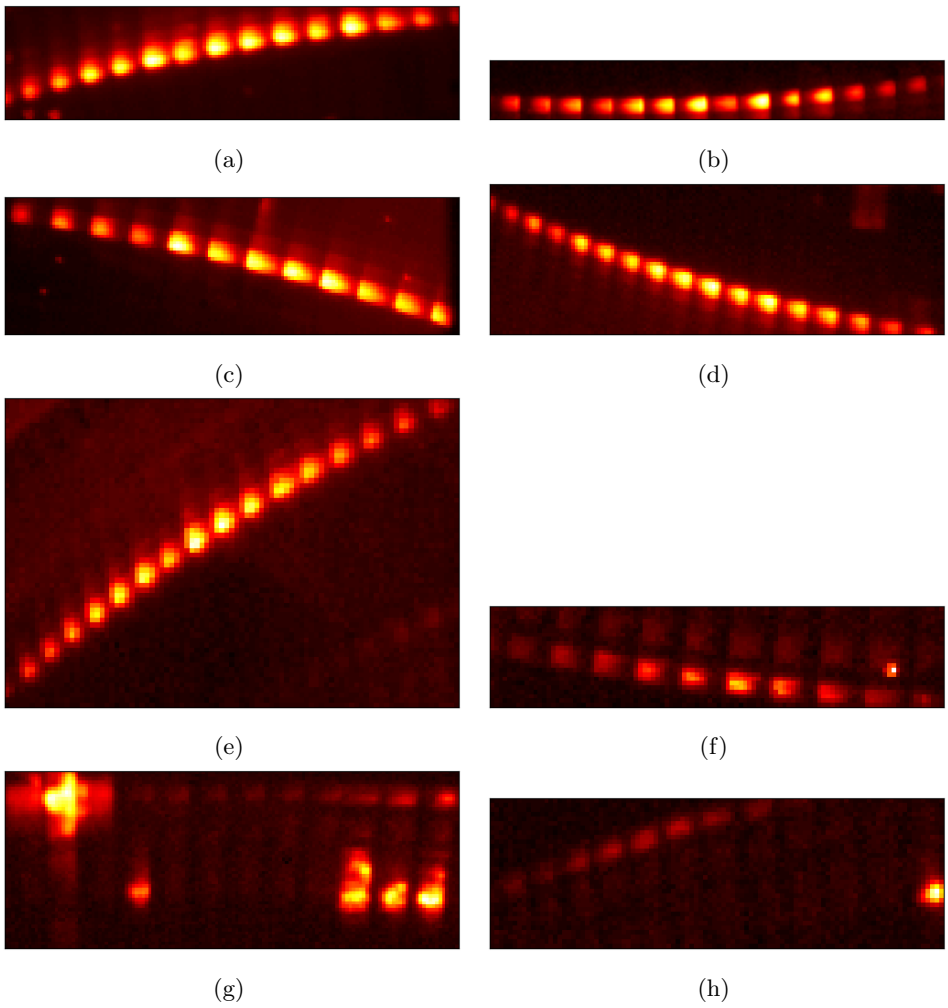

FIG. 8. Examples of good classifications on real images from C7 campaign (February/March 2023).
Non anomaly for (a),(b),(c),(d),(e) and with anomaly for (f),(g),(h).
"Hot" colormap for (a): [82°C;243°C], (b): [94°C;238°C], (c): [79°C;284°C], (d): [77°C;245°C], (e): [77°C;245°C], (f): [91°C;331°C], (g): [85°C;243°C], (h): [94°C;238°C].

	Accuracy	Recall	Precision	F1-score	Average calculation time / image
CNN *train on 130 real images*	0.82	0.11	**1**	0.20	0.002 s
CNN *train on 966 synthetic images*	0.47	0.11	0.05	0.08	0.09 s
SVM *train on 130 real images*	**0.87**	0.44	0.80	0.57	0.002 s
SVM *train on 966 synthetic images*	0.58	0.22	0.14	0.17	0.002 s
Max-tree method	**0.87**	**0.89**	0.62	**0.73**	0.46 s

TABLE V. Comparative table of the different methods on the test dataset (composed of 45 real-world images)

Recall is a metric that quantifies how many anomalies are correctly detected by the model among all the existing anomalies. It is crucial for anomaly detection because it indicates how responsive and exhaustive the model is in identifying abnormal patterns or behaviours that may suggest security threats or risks. In this aspect max-tree based method far outperforms the other techniques, which is consistent with all the criteria choices made beforehand.

It is important to emphasize that the max-tree classifier presented in this study does not require any training data. This eliminates issues related to the scarcity of labelled data. During experiments on the WEST tokamak, terabytes of data are captured by IR cameras; however, manual labelling of this data is a labour-intensive process. As such, the development of image classifica-

tion/regression techniques that uses only prior knowledge formulated as high level prescription is highly desirable. Such use of well formulated prior knowledge allow sparing the making of an extensive annotated database.

The max tree method takes significantly longer than the CNN and SVM methods (counting only the inference time, that is, excluding training time in this evaluation). The max-tree calculation time is still compatible with an off-line processing of the bounding boxes, between two experiments at WEST.

V. LIMITS OF APPLICABILITY

A. Study of physical parameters with the synthetic dataset

This section explores the sensitivity of max-tree classifier, applied to the parameter of vertical misalignment. The vertical misalignment is used here as the controlling parameter, and is representative of other possible overheating causes. 1350 synthetic images are available by varying three physical and structural parameters of the system, as already described in subsection III.A. This dataset of 1350 images is presumed to contain only strikelines with misalignments.

The dataset of 1350 images is classified using the present max-tree classifier on all this dataset. The proportion of abnormal vs normal strikeline is plotted in Figure 9(a), as a function of the vertical misalignment (unknown to the max-tree classifier). The plot shows a transition at a misalignment of 0.45 mm : beneath a misalignment of 0.45 mm, the classifier finds a majority of normal strikelines. Above 0.45 mm, the classifier find predominantly abnormal strike lines. More than 90% of images are classified as anomaly for a misalignment of 0.6mm.

This transition of 0.45 mm is commensurate with the PFU assembly tolerance of 0.3 mm, below which detecting an anomaly becomes challenging. The results of this study indicate that the proportion as a function of misalignment is consistent with previous physical studies conducted on the divertor assembly. It was observed that a misalignment of 0.3mm resulted in minimal discernible changes to the strikeline structure.

B. Practical case not detected by the max-tree method

Figure 9(b) highlights another observation consistent with the max-tree method's definition, the anomaly detection is independent of the misaligned PFU's location within the stripe. The max-tree method does not account for the spatial arrangement of the image pixels. It only provides information about the number and distribution of hot spots within each region. Therefore, the max-tree classifier may fail to detect a new hot spot that has similar characteristics as the typical hot spots in the strikeline region. To illustrate this issue, some synthetic and real images are presented and their classification is analysed.

A synthetic strikeline is modified by adding a zone with the same temperature distribution and maximum value as the centre of the original strikeline (Figure 5). This added hot spot is located in an area that a human expert identifies as anomalous, even though it is not particularly hot compared to the strikeline temperature.

This strikeline is classified as "normal". Max-tree method fails to detect a new region/shape that has the same temperature distribution and maximal temperature as the "central" strikeline. A concern is that this area can be potentially hot and damage a component of the machine. The reason for this misclassification is that the max-tree classifier only triggered one anomaly criterion (the branch size) in this case. The other two criteria (the maximum temperature and the distribution) are similar to those of other branches and the value is within the "3σ" rule. Therefore, the max-tree classifier does not recognize this region as an anomaly.

Few situations are encountered where the max-tree classifier fails to detect an anomalous strikeline in an infrared image of a tokamak plasma. Figure 10 shows an example of such an image, which is classified as normal by the max-tree classifier. However, a human expert considers it to be an anomaly because of the two small hot spots on the bottom and the right of the image. These hot spots are spacially distant from the strikeline but have similar features in terms of distribution and maximum temperature. Moreover, their shape resembles the hot zones in the centre of the strikeline. Therefore, the max-tree algorithm generates branches that are similar to the strikeline branches. The algorithm does not distinguish them from the aligned ones, based on the criteria established earlier. This real image illustrates the special case of a limitation of the proposed method.

To summarize, the max-tree classifier detects an anomaly if:

1. The anomaly has one or more pixels that are significantly hotter than the strikeline (this may trigger both the max temperature and distribution criteria).

2. The anomaly has a different distribution than the strikeline by having a very short or long spread (see distribution curves). This triggered the size and distribution criteria.

The result from this developing the max-tree classifier drawn is that it requires an anomaly to differ in its internal structure to be detected. The max-tree method does not consider the spatial position of the anomaly on the image/tokamak. In summary, the successful detection of anomalies using the proposed method relies on the structural differentiation ([1] or [2]) of the zone from the rest of the strikeline. A potential idea for future research could involve incorporating an additional brick to

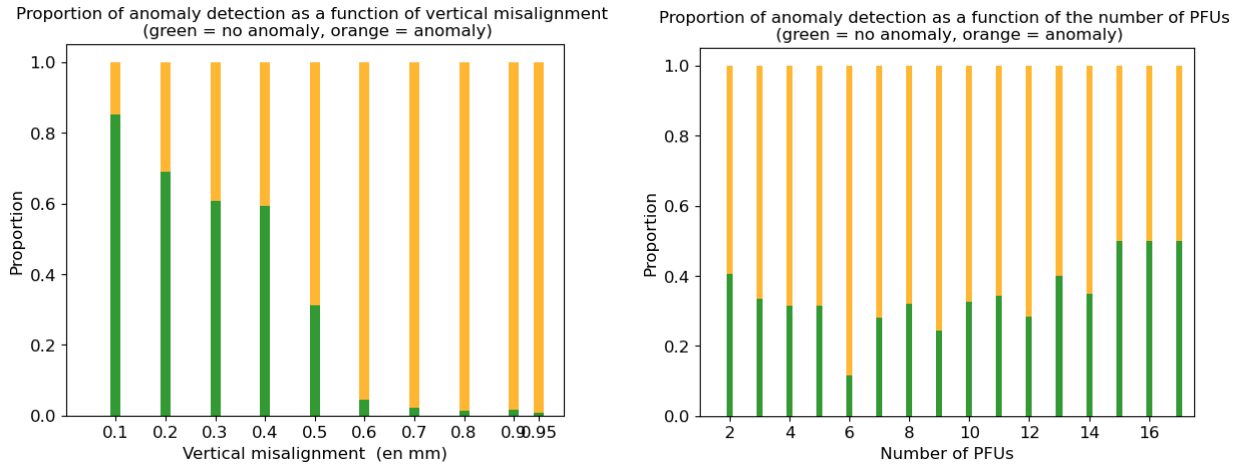

(a) (b)

FIG. 9. Proportion of anomaly/non anomaly detection in function of misalignment (a) and position of the anomaly (b). (Green for non anomaly and orange for anomaly)

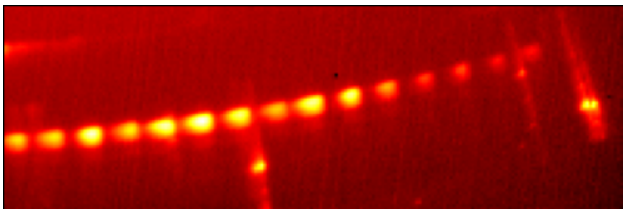

FIG. 10. Pulse 57541 - Camera DIVQ6A
("Hot" Colormap: [104°C;251°C])

the method, which would perform a secondary check by analysing the pixel's position within the image. However, this would necessitate additional information, such as the correspondence between pixel and position within the tokamak, which is currently an ongoing area of research within the laboratory.

However, experienced human experts who are responsible for the machine's safety identified most of the anomalies as belonging to case [1] and/or case [2].

VI. CONCLUSION

This article presents a novel method for hot spot classification on IR images of WEST tokamak using the max-tree image transformation method. The max-tree classifier is applied to the classification of strikeline anomalies which are, hot spots naturally present on the divertor of the WEST tokamak. The max-tree image processing method is coupled with criteria based on physical a-priori knowledge of the hot spot to perform this classification. The approach demonstrates an accuracy of 88% and a recall of 0.89 on real images compared to 87% (recall 0.44) and 82% (recall 0.11) for SVM and CNN respectively. Moreover, the max-tree classifier does not require labelled data. This is a significant advantage considering the complexity and time required to generate a labelled dataset from real data.

The generalisation of the max-tree based classification method for the entire first wall could involve the incorporation of a priori knowledge into deep learning models. Developing further this concept, the max-tree based classification method could be used to build a large databases of real images linked to geometrical structure of their hot spots.

ACKNOWLEDGEMENTS

The authors thanks Aleix Puig Sitges from Max-Planck-Institut für Plasmaphysik, and Dr Josep R. Casas and Pr Philippe Salembier from Universitat Politècnica de Catalunya, for introducing the max-tree image transformation technique, and the valuable discussions as well as for their collaboration and support in this work generally.

This work has been carried out within the framework of the EUROfusion Consortium, funded by the European Union via the Euratom Research and Training Programme (Grant Agreement No 101052200 — EUROfusion). Views and opinions expressed are however those of the author(s) only and do not necessarily reflect those of the European Union or the European Commission. Neither the European Union nor the European Commission can be held responsible for them.

DATA AVAILABILITY

The data that support the findings of this study are available on request from the corresponding author. The data are not publicly available due to privacy restriction.

REFERENCES

[1] J. Bucalossi *et al.*, "Operating a full tungsten actively cooled tokamak: overview of WEST first phase of operation," Nuclear Fusion **62**, 042007 (2022), publisher: IOP Publishing.

[2] G. Arnoux *et al.*, "A protection system for the JET ITER-like wall based on imaging diagnostics," Review of Scientific Instruments **83**, 10D727 (2012), publisher: American Institute of Physics.

[3] M. W. Chen, X. F. Yang, X. Z. Gong, K. F. Gan, B. Zhang, and Z. D. Yang, "Integrated infrared and visible tangential wide-angle viewing systems for surface temperature measurement and discharge monitoring in EAST," Fusion Engineering and Design **150**, 111415 (2020).

[4] A. Sitjes, M. Jakubowski, A. Ali, P. Drewelow, V. Moncada, F. Pisano, T. Ngô, B. Cannas, J.-M. Travere, G. Kocsis, T. Szepesi, and T. Szabolics, "Wendelstein 7-X Near Real-Time Image Diagnostic System for Plasma-Facing Components Protection," Fusion Science and Technology **74**, 1–9 (2017).

[5] B. Jabłoński, D. Makowski, P. Perek, P. Nowak vel Nowakowski, A. P. Sitjes, M. Jakubowski, Y. Gao, A. Winter, and T. W.-X. Team, "Evaluation of NVIDIA Xavier NX Platform for Real-Time Image Processing for Plasma Diagnostics," Energies **15**, 2088 (2022), number: 6 Publisher: Multidisciplinary Digital Publishing Institute.

[6] R. Clemente, *Detection and Classification of Thermal Events in the Wendelstein 7-X*, Master's thesis, Universitat Politècnica de Catalunya (2020).

[7] E. Urbach, J. Roerdink, and M. Wilkinson, "Connected Shape-Size Pattern Spectra for Rotation and Scale-Invariant Classification of Gray-Scale Images," IEEE transactions on pattern analysis and machine intelligence **29**, 272–85 (2007).

[8] X. Courtois, M. Aumeunier, C. Balorin, J. B. Migozzi, M. Houry, K. Blanckaert, Y. Moudden, C. Pocheau, A. Saille, E. Hugot, M. Marcos, and S. Vives, "Full coverage infrared thermography diagnostic for WEST machine protection," Fusion Engineering and Design SI:SOFT-30, **146**, 2015–2020 (2019).

[9] V. Martin, V. Moncada, G. Dunand, Y. Corre, E. Delchambre, and J. M. Travere, "Integrated software for imaging data analysis applied to edge plasma physic and operational safety," Fusion Engineering and Design **86**, 270–278 (2011).

[10] V. Martin, G. Dunand, V. Moncada, M. Jouve, and J.-M. Travere, "New field programmable gate array-based image-oriented acquisition and real-time processing applied to plasma facing component thermal monitoring," Review of Scientific Instruments **81**, 10E113 (2010), publisher: American Institute of Physics.

[11] V. Martin, J.-M. Travere, F. Bremond, V. Moncada, and G. Dunand, "Thermal Event Recognition Applied to Protection of Tokamak Plasma-Facing Components," IEEE Transactions on Instrumentation and Measurement **59**, 1182–1191 (2010), conference Name: IEEE Transactions on Instrumentation and Measurement.

[12] R. Mitteau, C. Belafdil, C. Balorin, X. Courtois, V. Moncada, R. Nouailletas, and B. Santraine, "WEST operation with real time feed back control based on wall component temperature toward machine protection in a steady state tungsten environment," Fusion Engineering and Design **165**, 112223 (2021).

[13] E. Grelier, R. Mitteau, and V. Moncada, "Deep learning and image processing for the automated analysis of thermal events on the first wall and divertor of fusion reactors," Plasma Physics and Controlled Fusion **64**, 104010 (2022), publisher: IOP Publishing.

[14] E. Grelier, R. Mitteau, and V. Moncada, "Deep learning-based process for the automatic detection, tracking, and classification of thermal events on the in-vessel components of fusion reactors," Fusion Engineering and Design **192**, 113636 (2023).

[15] J. Ahmed, B. Gao, and W. l. Woo, "Sparse Low-Rank Tensor Decomposition for Metal Defect Detection Using Thermographic Imaging Diagnostics," IEEE Transactions on Industrial Informatics **17**, 1810–1820 (2021), conference Name: IEEE Transactions on Industrial Informatics.

[16] H. Wang, S.-J. Hsieh, X. Zhou, B. Peng, and B. Singh, "Using active thermography to inspect pin-hole defects in anti-reflective coating with k-mean clustering," NDT & E International **76**, 66–72 (2015).

[17] P. C. Stangeby, *The Plasma Boundary of Magnetic Fusion Devices* (CRC Press, Boca Raton, 2000).

[18] T. Hirai, V. Barabash, F. Escourbiac, A. Durocher, L. Ferrand, V. Komarov, and M. Merola, "ITER divertor materials and manufacturing challenges," Fusion Engineering and Design **125**, 250–255 (2017).

[19] "Homepage | Cast3M http://www-cast3m.cea.fr/," .

[20] T. Eich, A. Leonard, R. Pitts, W. Fundamenski, R. Goldston, T. Gray, A. Herrmann, A. Kirk, A. Kallenbach, O. Kardaun, A. Kukushkin, B. LaBombard, R. Maingi, M. Makowski, A. Scarabosio, B. Sieglin, J. Terry, A. Thornton, ASDEX Upgrade Team, and JET EFDA Contributors, "Scaling of the tokamak near the scrape-off layer H-mode power width and implications for ITER," Nuclear Fusion **53**, 093031 (2013).

[21] P. Salembier, A. Oliveras, and L. Garrido, "Antiextensive connected operators for image and sequence processing," IEEE transactions on image processing : a publication of the IEEE Signal Processing Society **7**, 555–70 (1998).

[22] K. E. Purnama, M. H. F. Wilkinson, A. G. Veldhuizen, J. Lubbers, T. A. Sardjono, and G. J. Verkerke, "Branches filtering approach for max-tree," (2007).

[23] R. Souza, L. Tavares, L. Rittner, and R. Lotufo, "An Overview of Max-Tree Principles, Algorithms and Applications," in *2016 29th SIBGRAPI Conference on Graphics, Patterns and Images Tutorials (SIBGRAPI-T)* (IEEE, Sao Paulo, Brazil, 2016) pp. 15–23.

[24] E. Carlinet and T. Geraud, "A Comparative Review of Component Tree Computation Algorithms," IEEE Transactions on Image Processing **23**, 3885–3895 (2014).

[25] N. Sharma, V. Jain, and A. Mishra, "An Analysis Of Convolutional Neural Networks For Image Classification," Procedia Computer Science International Conference on Computational Intelligence and Data Science, **132**, 377–384 (2018).

[26] A. Krizhevsky, I. Sutskever, and G. E. Hinton, "ImageNet Classification with Deep Convolutional Neural Networks," in *Advances in Neural Information Processing Systems*, Vol. 25 (Curran Associates, Inc., 2012).

[27] J. Cervantes, F. Garcia-Lamont, L. Rodríguez-Mazahua, and A. Lopez, "A comprehensive survey

on support vector machine classification: Applications, challenges and trends," Neurocomputing **408**, 189–215 (2020).